

# On the variability of atmospheric $^{222}\text{Rn}$ activity concentrations measured at Neumayer, coastal Antarctica

R. Weller<sup>1</sup>, I. Levin<sup>2</sup>, D. Schmithüsen<sup>2</sup>, M. Nachbar<sup>2</sup>, J. Asseng<sup>1</sup>, and D. Wagenbach<sup>2</sup>

[1] Alfred Wegener Institute for Polar and Marine Research, Am Handelshafen 12, D-27570 Bremerhaven, Germany

[2] Institut für Umweltp Physik, Heidelberg University, Im Neuenheimer Feld 229, D-69120 Heidelberg, Germany

## Abstract

We report on continuously measured  $^{222}\text{Rn}$  activity concentrations in near surface air at Neumayer Station in the period 1995 through 2011. This 17 years record showed no long-term trend and has overall mean  $\pm$  standard deviation of  $(0.019\pm 0.012)$  Bq m<sup>-3</sup>. A distinct and persistent seasonality could be distinguished with maximum values of  $(0.028\pm 0.013)$  Bq m<sup>-3</sup> from January through March and minimum values of  $(0.015\pm 0.009)$  Bq m<sup>-3</sup> from May through October. Elevated  $^{222}\text{Rn}$  activity concentrations were typically associated with air mass transport from the Antarctic Plateau. Our results do not support a relation between enhanced  $^{222}\text{Rn}$  activity concentrations at Neumayer and cyclonic activity or long-range transport from South America. The impact of oceanic  $^{222}\text{Rn}$  emissions could not be properly assessed but we tentatively identified regional sea ice extent (SIE) variability as a significant driver of the annual  $^{222}\text{Rn}$  cycle.

## 1 Introduction

The radioactive noble gas Radon, specifically the isotopes  $^{222}\text{Rn}$  and  $^{220}\text{Rn}$  are the sole gaseous progenies of the  $^{238}\text{U}$  and  $^{232}\text{Th}$  radioactive series, respectively. Both natural actinides

28 are trace elements omnipresent in all minerals and soils (Nazaroff, 1992).  $^{222}\text{Rn}$  is a direct  
29 product of the  $\alpha$ -decay of  $^{226}\text{Ra}$  about a factor of  $10^{-4}$  less abundant in surface ocean waters  
30 compared to terrestrial soils (Wilkening and Clements, 1975) making the ocean to an only  
31 minor  $^{222}\text{Rn}$  source. From these global surface sources, the gaseous decay product  $^{222}\text{Rn}$  (and  
32 to a lesser extent  $^{220}\text{Rn}$  because of its much shorter radioactive half-life time  $T_{1/2}$  of 56 s  
33 compared to 3.82 d for  $^{222}\text{Rn}$ ) are continuously emitted into the atmosphere. Apart from local  
34 mineralogy and element composition of the soil, continental emission rates depend on soil  
35 texture and soil humidity and typically range between  $0.005\text{-}0.050\text{ Bq m}^{-2}\text{ s}^{-1}$  (Nazaroff, 1992;  
36 Karstens et al., 2013), about 2 orders of magnitude higher than oceanic emissions (e.g. Schery  
37 and Huang, 2004). For the latter a recent study derived from long-term  $^{222}\text{Rn}$  observation at  
38 Cape Grim (Tasmania) an oceanic  $^{222}\text{Rn}$  emission rate around  $2.7\times 10^{-4}\text{ Bq m}^{-2}\text{ s}^{-1}$   
39 (Zahorowski et al., 2013).

40 There are three main issues attracting some attention to atmospheric  $^{222}\text{Rn}$ , usually specified  
41 as activity concentrations in units of  $\text{Bq m}^{-3}$ : (i) Being an  $\alpha$ -emitter,  $^{222}\text{Rn}$  is a potential health  
42 hazard, particularly in certain regions with elevated  $^{226}\text{Ra}$  occurrence and in poorly ventilated  
43 buildings built with  $^{226}\text{Ra}$  rich stonework (Nazaroff, 1992). (ii) In terms of atmospheric  
44 chemistry, ionizing radiation emanated from  $^{222}\text{Rn}$  entails ion mediated particle nucleation,  
45 preferentially within the continental planetary boundary layer (Harrison and Carslaw, 2003;  
46 Hirsikko et al., 2011; Zhang et al., 2011). There,  $^{222}\text{Rn}$  could exceed the impact of cosmic  
47 radiation on particle nucleation (Zhang et al., 2011). (iii) Considering the relatively short  
48 radioactive half-life of 3.82 d combined with chemical inertness, atmospheric and radioactive  
49 lifetime of  $^{222}\text{Rn}$  are identical. Hence,  $^{222}\text{Rn}$  is a virtually ideal atmospheric tracer: on smaller  
50 spatial scales, turbulent vertical mixing within the troposphere (especially within the PBL)  
51 and soil emission fluxes have been assessed (Liu et al., 1984; Levin et al., 2002; Slemr et al.,  
52 2013), and on a larger, e.g. continental scale long range transport and air mass history could  
53 be derived from  $^{222}\text{Rn}$  measurements (e.g. Law et al., 2010). Due to these attributes, observed  
54 atmospheric  $^{222}\text{Rn}$  activity concentrations were frequently used to validate global atmospheric  
55 circulation models (e.g. Jacob et al., 1997). Basically all these applications of atmospheric  
56  $^{222}\text{Rn}$  activity concentrations broadly presume negligible oceanic  $^{222}\text{Rn}$  emissions.  
57 Interestingly, in a recent study long-term  $^{222}\text{Rn}$  observations from the remote station Cape  
58 Grim were employed to derive oceanic  $^{222}\text{Rn}$  emission rates by carefully screening the data

59 set, mainly with the help of a thorough backward trajectory analysis (Zahorowski et al.,  
60 2013). In addition, Taguchi et al. (2013) assessed  $^{222}\text{Rn}$  air-sea transfer rates derived from  
61 ship borne  $^{222}\text{Rn}$  measurements with the help of a global atmospheric transport model. Both  
62 approaches illustrated that in certain remote marine regions the impact of marine  $^{222}\text{Rn}$   
63 emissions may be decisive. Among such regions, notably Antarctica and the surrounding  
64 Southern Ocean has to be considered, particularly with regard to the fact that the ice covered  
65 Antarctic continent is virtually free from  $^{222}\text{Rn}$  emissions. Moreover, due to the fact that air-  
66 sea exchange is highly dependent on surface wind velocity, specifically the stormy Southern  
67 Ocean could be a significant  $^{222}\text{Rn}$  source (Schery and Huang, 2004, Taguchi et al., 2013).  
68 Previous measurements from that region revealed extremely low  $^{222}\text{Rn}$  activity concentrations  
69 (Maenhaut et al., 1979; Polian et al., 1986; Pereira, 1990; Lambert et al., 1990; Wyputta,  
70 1997, Ilić et al., 2005), which may be hypothetically consistent with recently ascertained  
71 marine emissions there (Zahorowski et al., 2013). Modelling studies by Heimann et al. (1990)  
72 predicted for instance in case of Neumayer a contribution of oceanic  $^{222}\text{Rn}$  emissions to be  
73 around 28% (derived from Table 2 therein). Nevertheless, data evaluation and discussion  
74 presented in previous studies implied that back ground  $^{222}\text{Rn}$  activity concentrations in this  
75 region were mainly determined by long-range transport from continental region, i.e. for the  
76 Atlantic sector of Antarctica dominantly from South America (Polian et al., 1986; Pereira,  
77 1990; Lambert et al., 1990; Wyputta, 1997). Observed spikes in  $^{222}\text{Rn}$  activity concentrations,  
78 so-called radon-storms frequently exceeding background activity concentrations by about an  
79 order of magnitude for several hours, were usually attributed to efficient long-range transport  
80 by cyclonic activity from South America (Polian et al., 1986; Wyputta, 1997). Apart from an  
81 only local impact of Antarctic  $^{222}\text{Rn}$  emissions from very few ice free regions situated mainly  
82 on the Antarctic Peninsula (Pereira, 1990) but probably also in coastal dry valleys and high  
83 mountain ranges, recent investigations of Taguchi et al. (2013) suggested a perceptible  
84 contribution of these sources for the remote Southern Ocean. However, considering the  
85 extremely small all-up area of insularly distributed rocky places in continental Antarctica, this  
86 appears somewhat arguable.

87 In this paper we present an analysis of long-term  $^{222}\text{Rn}$  activity concentrations recorded  
88 continuously at the German Antarctic Station Neumayer (NM) from 1995 through 2011. We  
89 shall discuss the variability of this time series on different timescales, especially focussing on

90 its distinct seasonality. The central topic guiding us through the analysis is the question to  
91 what extent marine, in contrast to continental  $^{222}\text{Rn}$  emissions, were responsible for the  
92 observed variability, bearing in mind that marine  $^{222}\text{Rn}$  emissions should be decisively  
93 governed by the seasonal wax and wane of sea ice. Our evaluation is further supported by  
94 local meteorological observations, backward trajectories, sea ice extent records and finally  
95 long-term  $^{210}\text{Pb}$  measurements (Elsässer et al., 2011), a  $^{222}\text{Rn}$  progeny with a half-life time  $T_{1/2}$   
96 = 22.3 y.

97

## 98 **2 Experimental techniques and data evaluation methods**

### 99 **2.1 Site description**

100  $^{222}\text{Rn}$  measurements were conducted during the period 1995 through 2011 at the Air  
101 Chemistry Observatory, Neumayer Station (70°39'S, 8°15'W,  
102 [http://www.awi.de/en/go/air\\_chemistry\\_observatory](http://www.awi.de/en/go/air_chemistry_observatory)). A map of all relevant stations here  
103 discussed is shown in Fig. 1. Neumayer is located on an ice shelf about 10 km away from the  
104 ice shelf edge. Apart from open water or seasonal sea ice cover the surroundings are totally  
105 ice covered and the nearest insular rocky outcrops are more than 200 km away. In several  
106 papers, the measuring site, meteorological conditions, contamination free sampling were  
107 already described in-depth and we just refer here in particular to Wagenbach et al. (1988),  
108 König-Langlo et al. (1998) and Weller et al. (2008, 2011a, and 2011b). Due to snow  
109 accumulation the observatory has to be typically jacked up every 2 years and hence the  
110 sampling high (inlet) varied between 6 m and 8 m above ground.

### 111 **2.2 Atmospheric $^{222}\text{Rn}$ activity measurements**

112 The activity concentration of the noble gas  $^{222}\text{Rn}$  was indirectly determined by measuring the  
113 activity of the short-lived metallic daughters, namely  $^{218}\text{Po}$  ( $T_{1/2} = 3$  min) and  $^{214}\text{Po}$  ( $T_{1/2} = 162$   
114  $\mu\text{s}$ ) which are attached to sub- $\mu\text{m}$  aerosol particles immediately after generation  
115 (Porstendörfer, 1994). We used a well-established home-made  $^{222}\text{Rn}$  monitor based on the  
116 static filter method (Levin et al., 2002). In short, the basic components of this monitor  
117 comprised an adapted filter holder equipped with quartz fibre filter (Whatman QMA,  $\varnothing$  47  
118 mm), an  $\alpha$ -detector with pre-amplifier and required data acquisition electronics. A

119 continuously monitored flow of ambient air was pumped through the quartz filter, enabling a  
120 complete interception of all particle-bound  $^{222}\text{Rn}$  progenies. At the same time, the overlapping  
121  $\alpha$  activity spectra of  $^{218}\text{Po}$  ( $\alpha_E = 6.0$  MeV) and  $^{214}\text{Po}$  ( $\alpha_E = 7.7$  MeV), were measured in situ  
122 with a surface barrier detector (Canberra CAM AB 900 mm<sup>2</sup> active surface, energy resolution  
123 50 keV at 5.486 MeV). At NM, the mean  $\alpha$ -activity of the  $^{222}\text{Rn}$  daughters was determined in  
124 3-hour intervals. From the measured  $^{214}\text{Po}$  activity we then estimated the atmospheric  $^{222}\text{Rn}$   
125 activity concentration, assuming radioactive equilibrium between  $^{222}\text{Rn}$  and its daughter  $^{214}\text{Po}$ .  
126 The overall accuracy of our  $^{222}\text{Rn}$  activity concentrations measured at NM was estimated to  
127 be about  $\pm(25-30)\%$ . This estimate includes the uncertainties of flow rate, detection noise and  
128 counting statistics as well as the potential disequilibrium between  $^{222}\text{Rn}$  and  $^{214}\text{Po}$ . For the  
129 latter, we considered the fact that disequilibrium effects were not determined at NM. The  
130 reproducibility of our measurements at NM has been determined to better than 15% based on  
131 parallel measurements of two independent monitors over a period of more than six months.  
132 Continuous  $^{222}\text{Rn}$  observation started at NM already in February 1983. The respective data set  
133 prior to 1995 is not included here, since the assimilation of the counts has been achieved via  
134 pre-set energy windows rather than ADC based spectrum assay. The lower quality in the raw  
135 count data evaluation let us refrain from discussing the entire NM radon record, although  
136 mean  $^{222}\text{Rn}$  levels in the pre-1995 period are quite comparable to those presented here (see  
137 Wyputta, 1997).

### 138 **2.3 Evaluation methods and auxiliary data sources**

139 In order to study the origin of the advected air masses we rely on 10-days backward  
140 trajectories provided by the HYSPLIT 4.0 (Hybrid Single-Particle Lagrangian Integrated  
141 trajectory; [http://www.arl.noaa.gov/documents/reports/hysplit\\_user\\_guide.pdf](http://www.arl.noaa.gov/documents/reports/hysplit_user_guide.pdf)). For all  
142 trajectory calculations we used NCAR/NCEP reanalysis meteorological data with a spatial  
143 resolution of  $2.5^\circ \times 2.5^\circ$  (longitude  $\times$  latitude grid). Calculations were executed in one hour  
144 time steps. Due to the fact that vertical wind components in reanalysis data could be  
145 somewhat problematic especially for regions with sparse meteorological input data (like the  
146 Southern Ocean; Harris et al., 2005) all trajectories were calculated using the 3D wind fields  
147 of the reanalysis data as well as employing the isentropic approximation. There were  
148 significant differences between individual 10-days back trajectories calculated either under  
149 three dimensional (3D, wind vector from meteorological data) or isentropic approximation,

150 but the general advection characteristic on which our conclusions were finally based appeared  
151 robust. More information on the accuracy of back trajectory estimates can be found in a  
152 review by Stohl (1998). Therefore we conclude that the simple backward trajectory analyses  
153 used here are appropriate for our purpose, particularly with regard to the sparse underlying  
154 meteorological data for high southern latitudes. For the same reason the validity of back  
155 trajectories exceeding 10 days appeared little conclusive due to their large spatial uncertainty.

156 In contrast to ice-free terrestrial surfaces, the Antarctic continent can be regarded as virtually  
157  $^{222}\text{Rn}$  source-free, more precisely  $^{222}\text{Rn}$  emissions are restricted to few outcropping rocks (so-  
158 called nunataks) especially on the Antarctic Peninsula, bare soil and rocky terrains at the  
159 coastal ice edge and in Dry Valleys. Irrespective of the fact that the surface could be a  $^{222}\text{Rn}$   
160 source or sink (the latter for particle bound  $^{222}\text{Rn}$  progenies), the characteristics of the  
161 boundary layer, in particular the depth of the mixing layer co-determines the actually  
162 measured atmospheric  $^{222}\text{Rn}$  activity concentration. Surface inversions are prevalent in  
163 Antarctica extending up to about 2 km during winter while from November to February  
164 inversions are rare and confined to heights of less than 1 km (König-Langlo et al., 1998).  
165 However, for most of the time an at least moderately stable boundary layer (SBL) is present,  
166 whose thickness can be estimated as the lowest altitude above ground where the vertical heat  
167 flux ceased to a small fraction of its surface value (typically 5%, Caughey et al., 1979).  
168 According to Handorf (1996) the SBL at NM typically ranged between 10 m and 50 m  
169 consistent with tether sondes and sodar results from Halley Station (Anderson and Neff, 2008;  
170 Jones et al., 2010), like NM a site on the ice shelf with comparably flat surface topography.  
171 Although vertical mixing depth is not well characterized in a SBL (Anderson and Neff, 2008),  
172 we tried to gauge vertical mixing in that layer like in Weller et al. (2011a) by using the local  
173 bulk Richardson number (Stull, 1988):

174

$$Ri_B = \frac{g \Delta\theta / \Delta z}{\theta \left[ \left( \frac{\Delta U}{\Delta z} \right)^2 + \left( \frac{\Delta V}{\Delta z} \right)^2 \right]} \quad (1)$$

175

176 with  $g$ , the gravitational constant ( $9.81 \text{ m/s}^2$ ),  $z$  the height above ground,  $\Theta$  the dry potential  
177 temperature,  $U$  and  $V$  the horizontal wind vectors in  $x$  and  $y$  direction, respectively. Gradients

178 where approximated by the difference of the measured temperatures and wind velocities at 2  
179 m and 10 m height. Note that at least for small Richardson numbers (well below 1.0), fluxes  
180 within the SBL appear to be a continuous function of  $Ri_B$  (Fernando and Weil, 2010,  
181 Mauritsen and Svensson, 2007).

182 Finally we used sea ice extent (SIE; i.e. sea ice area in units  $10^6 \text{ km}^2$ ) data from National  
183 Snow and Ice Data Center (NSIDC, <http://nsidc.org/>) with an original grid resolution of  
184  $25 \times 25 \text{ km}^2$  until 2002 and from then on  $6.25 \times 6.25 \text{ km}^2$ . Our analysis was based on a  
185 resampled data set with a longitudinal resolution of 10 degree (Weller et al., 2011b).

186

## 187 **3 Results**

### 188 **3.1 Data presentation**

189 Figure. 2 presents an overview of the daily mean  $^{222}\text{Rn}$  activity concentration time series  
190 continuously recorded between 1995 through 2011 at NM. In addition, monthly means of the  
191 time series are depicted in Fig. 3 (Supplementary data are available at  
192 <http://doi.pangaea.de/10.1594/PANGAEA.822027> ). At first glance, overall  $^{222}\text{Rn}$  levels at  
193 NM appeared constant throughout the observation period, with a long-term median of  $0.016$   
194  $\text{Bq m}^{-3}$  (mean =  $0.019 \text{ Bq m}^{-3}$ , standard deviation std. =  $0.012 \text{ Bq m}^{-3}$ ). Indeed, a statistical  
195 trend analyses, either by simple linear regression or non-parametric rank-order Mann-Kendall  
196 test with Sen's slope estimate (Hirsch et al., 1982) revealed no meaningful long-term trend.  
197 Nevertheless, there seems to be a broad and gentle maximum between 1998 and 2006,  
198 especially discernible in Fig. 3.

199 Apart from the latter rather marginal and yet unexplained finding, the salient feature is a  
200 striking seasonality with a maximum around austral summer (Fig. 4). This summer maximum  
201 appears uniformly each year between January and March with a mean  $\pm$  std of  $(0.028 \pm 0.013)$   
202  $\text{Bq m}^{-3}$  and these three months (JFM) will be henceforth defined as (local) "summer". A broad  
203 minimum of  $(0.015 \pm 0.009) \text{ Bq m}^{-3}$  emerged from May through October (MJJASO) and this  
204 period will be termed (local) "winter" throughout the paper. Finally we address here the  
205 variability on smaller timescale and inspect to this end the  $^{222}\text{Rn}$  time series in the highest  
206 available temporal resolution (3 h bins) separately for summer and winter; however, we  
207 cannot detect any significant diurnal cycle in either case.

## 208 3.2 Impact of local meteorology and long range transport

209 In contrast to aerosol-bound radionuclides like  $^{210}\text{Pb}$ , the sole  $^{222}\text{Rn}$  sink is radioactive decay  
210 which occurs homogeneously throughout a vertical air column while for the former a vertical  
211 gradient caused by the surface sink is typical. Taking into account that the ice shelf is  
212 definitely  $^{222}\text{Rn}$  source-free, a given  $^{222}\text{Rn}$  reservoir below a surface inversion layer should be  
213 more or less depleted by radioactive decay, provided this inversion layer is isolated from the  
214 atmosphere above. In this regard we have to consider that during summer a nocturnal  
215 inversion layer, largely preventing vertical mixing, could be frequently observed at NM.  
216 Regarding the radioactive decay time, we may barely expect a significant diurnal  $^{222}\text{Rn}$  cycle,  
217 since an even 12 h lasting surface inversion would at most cause 14%  $^{222}\text{Rn}$  depletion. This  
218 conclusion, which is consistent with our observations was further supported by an analysis in  
219 terms of PBL stability, assessed by bulk Richardson number  $\text{Ri}_B$  (accordingly defined as  
220 turbulent PBL for  $\text{Ri}_B < 0.25$  compared to laminar flow conditions for  $\text{Ri}_B > 1.0$ ). Concerning  
221 summer, no significant difference ( $p = 0.9$ ) in  $^{222}\text{Rn}$  activity concentrations could be verified  
222 between both stability cases ( $0.0279 \text{ Bq m}^{-3}$  compared to  $0.0283 \text{ Bq m}^{-3}$  for laminar and  
223 turbulent conditions, respectively). The situation is different for polar night where  $^{222}\text{Rn}$   
224 activity concentrations appeared significantly higher ( $p = 0.0002$ ) in a well-mixed, turbulent  
225 boundary layer ( $0.0157 \text{ Bq m}^{-3}$ ,  $N = 8726$ ) compared to laminar flow conditions ( $0.0135 \text{ Bq}$   
226  $\text{m}^{-3}$ ,  $N = 228$ ). During that period, vertical mixing should usually be much longer suppressed  
227 by persistent surface inversions, occasionally lasting for several days compared to only some  
228 hours during polar day. A more detailed inspection revealed, however, that distinct  $^{222}\text{Rn}$   
229 depletions events are rarely observed under such lasting stagnant flow condition, indicating  
230 that an effective isolation of near surface air masses at NM was usually not given.  
231 Nevertheless, we tentatively argue that on the whole, stagnant conditions (characterized by  
232  $\text{Ri}_B > 1$ ) probably caused on average appreciably lower  $^{222}\text{Rn}$  activity concentrations within  
233 the SBL during winter.

234 In a further attempt we examined the prevalent assumption that  $^{222}\text{Rn}$  rich air masses are  
235 efficiently advected by cyclonic activity from northerly continents (mainly South America in  
236 case of NM) towards Antarctica (Polian et al., 1986; Pereira, 1990; Wyputta, 1997). To this  
237 end we relied on long-term meteorological observations at NM (König-Langlo et al., 1998),  
238 and categorized the general weather situation into “marine cyclonic” with high wind

239 velocities  $>15 \text{ m s}^{-1}$  associated with easterly wind directions within the sector  $60^\circ\text{-}120^\circ$  in  
240 contrast to “continental”, characterized by low wind velocities  $<8 \text{ m s}^{-1}$  and southerly wind  
241 directions between  $140^\circ$  and  $200^\circ$ . Again, we examined  $^{222}\text{Rn}$  activity concentrations under  
242 these weather conditions separately for summer and winter. Contrary to our expectations,  
243 daily mean  $^{222}\text{Rn}$  activity concentrations were significantly higher ( $p < 10^{-88}$ ) under continental  
244 advection from the interior ice sheet during summer ( $0.0326 \text{ Bq m}^{-3}$ ,  $N = 5428$ , compared to  
245  $0.0246 \text{ Bq m}^{-3}$ ,  $N = 1972$  for marine cyclonic conditions), while for winter virtually no  
246 difference was discernible ( $p = 0.5$ ;  $0.0155 \text{ Bq m}^{-3}$  compared to  $0.0150 \text{ Bq m}^{-3}$  for continental  
247 and marine cyclonic conditions, respectively).

248 This rather simple evaluation was further supported by more detailed trajectory analyses. First  
249 we calculated 10-days backward trajectories for days with the 10 highest mean  $^{222}\text{Rn}$  activity  
250 concentrations (so-called radon storms) trying to identify long range transport from northward  
251 continents, especially South America. Surprisingly, the result presented in Fig. 5 did not show  
252 any “radon storm trajectory” originating from South America or any other northern continent.  
253 In a next attempt, the same procedure was done for the 10 lowest daily  $^{222}\text{Rn}$  activity  
254 concentrations (Fig. 6). In contrast to highest  $^{222}\text{Rn}$  events, lowest values could be observed  
255 throughout the year without a distinct seasonal preference. In conclusion, neither the highest  
256 nor the lowest observed  $^{222}\text{Rn}$  activity concentrations were linked with a characteristic  
257 advection scheme. In addition most of the shown trajectories implied long range transport.  
258 Considering in summary all daily trajectories in conjunction with the NM  $^{222}\text{Rn}$  time series,  
259 during summer 10-days backward trajectories related to low  $^{222}\text{Rn}$  events (below one std of  
260 the mean, i.e.  $<0.013 \text{ Bq m}^{-3}$ ,  $N = 139$ ) seem mainly localized at distances less than 1000 km  
261 to NM. Corresponding trajectories linked with elevated  $^{222}\text{Rn}$  activity concentrations (one std  
262 above of the mean, i.e.  $>0.043 \text{ Bq m}^{-3}$ ,  $N = 188$ ) frequently indicated long range transport  
263 (Fig. 7). Remarkably in this case, a large part of the trajectories move across the Antarctic  
264 plateau (Fig. 7a; blue region showing the highest relative number of trajectories intersecting  
265 with a  $1^\circ \times 1^\circ$  grid cell), contrary to the case low  $^{222}\text{Rn}$  conditions (Fig. 7b). Finally we note  
266 that immediate air mass transport from South America was found to be generally rare: Less  
267 than 5% of all 10 days backward trajectories eventually originated from this radon source  
268 region. Concerning winter, no meaningful differences in the trajectory pattern between high

269 (above one std of the mean, i.e.  $>0.023 \text{ Bq m}^{-3}$  in this case,  $N = 257$ ) and low (below one std of  
270 the mean, i.e.  $<0.007 \text{ Bq m}^{-3}$ ,  $N = 209$ )  $^{222}\text{Rn}$  activity concentrations were obvious (Fig. 8).

271 In summary, elevated  $^{222}\text{Rn}$  activity concentrations at NM tended to be typically linked with  
272 southerly air mass flow from the Antarctic Plateau and especially during winter, to a  
273 transiently turbulent (local) PBL. Based on our observations, the role of  $^{222}\text{Rn}$  emissions from  
274 ice free regions in Antarctica could not be assessed, though the fact that  $^{222}\text{Rn}$  levels at NM  
275 were comparable to the rocky site DDU cast into doubt a significant contribution of ice free  
276 regions. Surprisingly and in contrast to previous reporting on Antarctic radon (Antarctic  
277 Peninsula: Polian et al., 1986 and Pereira, 1990; NM data from 1984-1989: Wyputta, 1997),  
278 at least for summer  $^{222}\text{Rn}$  levels at NM appeared to be relatively low during stormy  
279 conditions, i.e. when NM was governed by northerly passing cyclones. As for winter, a  
280 cyclonic impact on  $^{222}\text{Rn}$  levels was not apparent at all.

281

## 282 **4 Discussion**

### 283 **4.1 Seasonal aspects: Impact of transport efficiency**

284 Previous measurements indicated that atmospheric  $^{222}\text{Rn}$  activity concentrations decrease  
285 distinctly from temperate regions of the Southern Ocean towards Antarctica (Polian et al.,  
286 1986, Lambert et al., 1990). Highest mean values were observed on the sub-polar sites Îles  
287 Crozet, Îles Kerguelen, and Amsterdam Island (annual mean around  $0.04 \text{ Bq m}^{-3}$ ). At these  
288 sites  $^{222}\text{Rn}$  time series were accompanied by a seasonal maximum between May and August  
289 (Polian et al., 1986). For coastal Antarctica annual mean  $^{222}\text{Rn}$  activity concentrations  
290 measured at Dumont d'Urville (DDU) appeared comparable to NM, but were about a factor of  
291 two lower at Mawson. Although the reported  $^{222}\text{Rn}$  seasonality at DDU and Mawson was  
292 similar to NM and characterized by a marked maximum during polar day (summer), the  
293 seasonal amplitude at Mawson was much lower (Polian et al., 1986, Lambert et al., 1990).  
294 Note, however, that the distinct discrepancy in the summer maximum between DDU and  
295 Mawson is not supported by more recent observations from the latter site (Zhang et al., 2011,  
296 Fig. 11 therein). At the Antarctic Peninsula (Vernadsky Station,  $65^{\circ}15'S$ ,  $64^{\circ}16'W$ ) the  $^{222}\text{Rn}$   
297 maximum was shifted to April (Ilić et al., 2005). Obviously,  $^{222}\text{Rn}$  seasonality at sub-  
298 Antarctic islands showed the exact opposite to those of coastal Antarctica. Lowest  $^{222}\text{Rn}$

299 levels were reported from South Pole (typically between 0.011–0.015 Bq m<sup>-3</sup>), but here the  
300 reported data set was too short to derive an annual cycle (Maenhaut et al., 1979). Different  
301 seasonality and higher <sup>222</sup>Rn levels within the temperate zone of the Southern Ocean  
302 compared to Antarctica has been explained by (i) a closer proximity to the northern source  
303 continents and (ii) efficient long-range transport from these sources by cyclonic activity  
304 peaking in the winter season (Polian et al., 1986). For Antarctica, on the other hand, the  
305 persistence of the surface inversion layer during polar night prevents down-mixing of air  
306 masses from northerly regions and shifts the seasonal maximum towards polar summer  
307 (Polian et al., 1986). These assumptions definitely neglected the impact of regional or even  
308 nearby oceanic <sup>222</sup>Rn emissions. Model simulations by Heimann et al. (1990) considering  
309 merely long-range <sup>222</sup>Rn transport from northerly continents to Antarctica essentially failed in  
310 describing the annual <sup>222</sup>Rn cycle observed at DDU.

311 In discussing the pronounced <sup>222</sup>Rn seasonality at NM, we have first to consider a potential  
312 impact of the disequilibrium between <sup>222</sup>Rn and the (measured) <sup>214</sup>Po activity, discussed by  
313 Levin et al. (2002), as well as a potential loss of un-attached <sup>222</sup>Rn progeny in the aerosol-  
314 based sampling system. The apparent resemblance of the mean <sup>222</sup>Rn seasonality (Fig. 4) with  
315 the mean annual cycle of condensation particle (CP) concentrations at NM (Weller et al.,  
316 2011a, Fig. 4 therein) suggests such an interference. Unlike the noble gas <sup>222</sup>Rn the metal  
317 <sup>214</sup>Po is attached to sub- $\mu$ m aerosol particles and hence the disequilibrium could be higher at  
318 low particle concentrations during winter. To clarify this point, we investigated the relation  
319 between CP concentrations and <sup>222</sup>Rn activity concentrations. The result is shown in Fig. 9.  
320 We calculated a Pearson correlation coefficient  $r$  to be 0.213 ( $r^2 = 0.045$ ;  $N = 42434$ ) for the  
321 highest available temporal resolution of the data (3-hour means), and somewhat higher for  
322 daily mean values ( $r^2 = 0.076$ ;  $N = 5365$ ). In addition we repeated the correlation analysis  
323 with corresponding monthly anomalies of the measured CP concentrations and <sup>222</sup>Rn activity  
324 concentrations (for calculation of anomalies see Weller et al., 2011b). No statistically  
325 significant correlation ( $r^2 = 0.02$ ,  $p = 0.084$ ;  $N = 206$ ) could be detected in this case. We  
326 reason that at most less than about 7.6% of the <sup>222</sup>Rn variability could be explained by CP  
327 concentration variability, excluding a relevant impact of particle number concentrations on  
328 observed <sup>222</sup>Rn activity (note that the peak to valley ratio of the annual <sup>222</sup>Rn cycle is around a  
329 factor of three). In addition we could not find any statistically significant impact of potentially

330 aerosol depleting weather conditions like snow drift, precipitation or (very rare) fog events on  
331 observed  $^{222}\text{Rn}$  activity concentrations at NM. Concerning inlet efficiency, test measurements  
332 indicate only minor  $^{222}\text{Rn}$  losses, typically within 5-10%.

333 Consequently other potential reasons for the observed  $^{222}\text{Rn}$  seasonality have to be examined.  
334 With the tentative assumption that in our case a southern hemispheric continent north of  
335 Antarctica is the main source region for atmospheric  $^{222}\text{Rn}$ , a comparison with the mean  
336 annual cycle of the following tracers and parameters also measured at NM appeared  
337 worthwhile and is summarized in Fig. 10: (a) the  $^{222}\text{Rn}$  progeny  $^{210}\text{Pb}$  (Elsässer et al., 2011),  
338 (b) the mineral dust tracer Lanthanum (La) for which the main source region is again South  
339 America (Weller et al., 2008), (c) the bulk Richardson number as a measure for boundary  
340 layer stability, and finally (d) SIE. Obviously, amplitude and narrow width of the seasonal  
341  $^{222}\text{Rn}$  maximum were clearly outstanding among all the other atmospheric tracers. Only  
342 regional SIE showed a strong and narrow minimum coinciding with the  $^{222}\text{Rn}$  maximum (Fig.  
343 10d).

344 A potential cause of the different seasonality observed for  $^{222}\text{Rn}$  and its progeny  $^{210}\text{Pb}$  could  
345 be wet and dry deposition, which is almost irrelevant for the noble gas  $^{222}\text{Rn}$  but crucial for  
346 the particle-bound  $^{210}\text{Pb}$  isotope. But from this point of view, it is hard to explain why  $^{210}\text{Pb}$   
347 was apparently much more efficiently depleted during mid-summer (JFM) compared to spring  
348 (Figs. 4 and 10a). The situation is different at DDU where  $^{222}\text{Rn}$  and  $^{210}\text{Pb}$  seasonality  
349 coincided as expected (Lambert et al., 1990). Similar to  $^{210}\text{Pb}$  the mineral dust tracer La  
350 showed at NM a rather broad annual cycle, in contrast to  $^{222}\text{Rn}$  and  $^{210}\text{Pb}$  (Figs. 4, 10a and  
351 10b). As discussed by Elsässer et al. (2011), the amplitude of La cycle was significantly  
352 higher most probably due to the stronger seasonality of the mineral dust source strength and  
353 higher atmospheric residence time of  $^{210}\text{Pb}$  compared to the primarily large mineral dust  
354 particles (Elsässer et al., 2011). Finally, the seasonality of boundary layer stability estimated  
355 by  $\text{Ri}_B$  appeared as the less pronounced and most dissimilar compared to  $^{222}\text{Rn}$  (Fig. 10c).  
356 Consequently, in terms of source strength and atmospheric transport efficiency we would  
357 expect a much broader and less pronounced seasonal  $^{222}\text{Rn}$  maximum at NM provided that  
358 South America was the main source region.

## 359 **4.2 Seasonal aspects: Impact of marine emissions and SIE**

360 There are marked similarities between the seasonality of  $^{222}\text{Rn}$  and SIE indicating oceanic  
361  $^{222}\text{Rn}$  emissions as main source. In this case only open water comes into consideration,  
362 because the ice shelf itself and also the sea ice covered ocean can be regarded as negligible  
363  $^{222}\text{Rn}$  sources. This source should be dominant during SIE minimum concurrently with the  
364 annual  $^{222}\text{Rn}$  summer maximum (Figs. 4 and 10d). Notwithstanding, a statistical analysis  
365 based on daily SIE data in  $10^\circ$  longitude resolution along with  $^{222}\text{Rn}$  activity concentrations  
366 generally revealed an only weak correlation. Regarding summer, the correlation between both  
367 parameters, calculated by a bivariate regression considering the uncertainties of both variables  
368 (Cantrell, 2008), was actually highest for the SIE sector  $20^\circ\text{E}$  to  $30^\circ\text{E}$  whereby about 8.1% ( $p$   
369  $<10^{-20}$ ) of the  $^{222}\text{Rn}$  variability could be explained by SIE variability (Fig. 11). For winter, we  
370 did not detect any significant correlation. Finally, we found an only minor impact of nearby  
371 oceanic  $^{222}\text{Rn}$  emissions (and consequentially local SIE variability): During summer, we  
372 measured definitely lower  $^{222}\text{Rn}$  activity concentrations under northerly flow conditions, i.e.  
373 advection from the open water ahead of NM (regarding daily means:  $0.0231 \text{ Bq m}^{-3}$  for  
374 northerly wind direction between  $300^\circ$  and  $60^\circ$ ,  $N = 293$  cases, compared to  $0.0286 \text{ Bq m}^{-3}$   
375 for remaining wind directions between  $60^\circ$  and  $300^\circ$ ,  $N = 9460$ ,  $p <10^{-7}$ ). Hence a significant  
376 influence of SIE modulated oceanic  $^{222}\text{Rn}$  emissions appeared arguable.

377 Nevertheless, considering and balancing all findings presented above, we tentatively suggest  
378 the regional SIE variability as a significant driver of the observed  $^{222}\text{Rn}$  seasonality. The  
379 moderate correlation between both parameters appears not so surprising, keeping in mind that  
380 oceanic  $^{222}\text{Rn}$  emission strength is (apart from SIE) highly dependent on surface wind  
381 velocity (Schery and Huang, 2004; Taguchi et al., 2013). Source strength and also transport  
382 efficiency associated with air mass history determined  $^{222}\text{Rn}$  activity concentrations  
383 eventually measured at NM. The impact of these different processes may have blurred an  
384 inherently more pronounced correlation with SIE data. Most probably the main oceanic  
385 source regions were some 1000 km away from NM as supported by trajectory analyses which  
386 indicate as well a main transport route via the Antarctic continent (Fig. 7a). In addition, the  
387 long transport routes indicated in Fig. 7a imply high wind velocities and efficient sea-air  
388 exchange processes. The exceptionally low  $^{222}\text{Rn}$  activity concentrations measured under  
389 advection from open water ahead of NM may be a consequence of the generally very low  
390 wind velocities ( $4\pm 3 \text{ m/s}$ ) and hence minimized sea-air exchange under these conditions.

391

## 392 **5 Conclusions**

393  $^{222}\text{Rn}$  activity levels measured at NM were in principle consistent with those observed at Cape  
394 Grim provided that the latter site was governed by advection of clean marine air masses.  
395 Following the arguments of Zahorowski et al. (2013), in such air masses  $^{222}\text{Rn}$  levels should  
396 be determined by marine emissions. This finding motivated the attractive hypothesis that also  
397  $^{222}\text{Rn}$  activity concentrations at NM and in particular their distinct seasonality may be largely  
398 caused by marine emissions and inherently linked with the annual cycle of SIE. In addition,  
399 sporadic radon storms should have been caused by long-range transport of continental air  
400 masses from South America. Actually, based on our present evaluation, a more complicated  
401 and somewhat ambiguous general view emerged. Although we could not properly assess the  
402 contribution of oceanic  $^{222}\text{Rn}$  emissions to the observed  $^{222}\text{Rn}$  activity concentrations at NM,  
403 we can state that the marine  $^{222}\text{Rn}$  source and the impact of SIE should be of significant  
404 importance in particular concerning the distinct seasonal maximum in February coinciding  
405 with the regional SIE minimum. Regarding trajectory analyses and local meteorology, there  
406 was a distinct difference during summer in air mass characteristics between high and low  
407  $^{222}\text{Rn}$  activity concentrations: High  $^{222}\text{Rn}$  activity concentrations were generally associated  
408 with long range transport, while advection during low  $^{222}\text{Rn}$  activity concentrations was more  
409 regionally confined (less than 1000 km ambit). Long range transport is typically associated  
410 with high wind velocities promoting sea-air exchange processes. Furthermore air masses with  
411 high  $^{222}\text{Rn}$  activity concentrations seem to arrive at NM preferentially via the Antarctic  
412 plateau, probably after down mixing of free tropospheric air masses. At first sight, these latter  
413 findings seem also to be consistent with the previously raised assumption that  $^{222}\text{Rn}$  activity at  
414 coastal NM should be governed by long-range air mass transport from South America and  
415 modulated by the efficiency of downward mixing into the PBL over Antarctica (Polian et al.,  
416 1986). Nevertheless, in our case the distinct seasonality of  $^{222}\text{Rn}$  levels (and especially the  
417 divergent annual cycle of  $^{210}\text{Pb}$  concentrations) could not satisfactorily be explained with it.  
418 At last we found that high  $^{222}\text{Rn}$  activity concentrations were usually not associated with  
419 cyclonic activities and on the whole, the impact of immediate long range transport from the  
420 South American continent emerged as marginal. Consequently, at least for NM but most  
421 probably also for other Antarctic sites, the usage of  $^{222}\text{Rn}$  activity concentrations to assess air

422 masses history remains ambiguous. To clarify this crucial point, there is a need for extensive  
423 measurements of vertical  $^{222}\text{Rn}$  profiles above Antarctica and the Southern Ocean, particularly  
424 under different general weather situations. Finally, one has to keep in mind that the validity of  
425 the presented backward trajectory analyses is somewhat limited. The use of more  
426 sophisticated dispersion models considering all available Antarctic  $^{222}\text{Rn}$  records should  
427 significantly improve our knowledge about processes governing the spatial and temporal  
428 variability of the Antarctic  $^{222}\text{Rn}$  inventory.

429

### 430 **Acknowledgements**

431 The authors would like to thank the many technicians and scientists of the Neumayer  
432 overwintering crews, whose outstanding commitment enabled achieving continuous, high  
433 quality aerosol and trace gas records since 1982. Special thanks go to Holger Schmithüsen  
434 and Gert König-Langlo for their effort in compiling meteorological data for our purpose. We  
435 are thankful to NOAA Air Resources Laboratory for having made available the HYSPLIT  
436 trajectory calculation program as well as all used input data files. We also acknowledge partly  
437 funding of the initial phase of the air chemical NM Observatory programme by the German  
438 Science Foundation (DFG) as well as financial support obtained within the European  
439 Community STEP program within the project Polar Atmospheric Chemistry.

440

441 **References**

- 442 Anderson, P. S. and Neff, W. D.: Boundary layer physics over snow and ice, *Atmos. Chem.*  
443 *Phys.*, 8, 3563-3582, doi:10.5194/acp-8-3563-2008, 2008.
- 444 Cantrell, C. A.: Technical Note: Review of methods for linear least-squares fitting of data and  
445 application to atmospheric chemistry problems, *Atmos. Chem. Phys.*, 8, 5477-5487,  
446 doi:10.5194/acp-8-5477-2008, 2008.
- 447 Caughey, S.J., Wyngaard, J.C., and Kaimal, J.C.: Turbulence in the Evolving Stable  
448 Boundary Layer, *J. Atmos. Sci.*, 6, 1041-1052, 1979.
- 449 Elsässer, C., Wagenbach, D., Weller, R., Auer, M., Wallner, A., and Christl, M.: Continuous  
450 25-years aerosol records at coastal Antarctica: Part 2: variability of the radionuclides  $^7\text{Be}$ ,  
451  $^{10}\text{Be}$  and  $^{210}\text{Pb}$ , *Tellus*, 63B, 920-934, doi: 10.1111/j.1600-0889.2011.00543.x, 2011.
- 452 Fernando, H.J.S. and Weil, J.C.: Whither the Stable Boundary Layer? A Shift in the Research  
453 Agenda, *Bull. Amer. Meteor. Soc.*, 91(11), 1475-1484, doi:10.1175/2010BAMS2770.1, 2010.
- 454 Handorf, D.: Zur Parametrisierung der stabilen atmosphärischen Grenzschicht über einem  
455 antarktischen Schelfeis, in *Reports on Polar and Marine Research*, 204, edited by F. Riemann,  
456 Alfred-Wegener-Inst. for Polar and Marine Res., Bremerhaven, 1996.
- 457 Harris, J.M., Draxler, R.R., and Oltmans, S.J.: Trajectory model sensitivity to differences in  
458 input data and vertical transport method, *J. Geophys. Res.*, 110, D14109,  
459 doi:10.1029/2004JD005750, 2005.
- 460 Harrison, R.G. and Carslaw, K.S.: Ion-aerosol-cloud processes in the lower atmosphere,  
461 *Reviews of Geophysics*, 41(3), 1012, doi:10.1029/2002RG000114, 2003.
- 462 Heimann, M., Monfray, P., and Polian, G.: Modeling the long-range transport of  $^{222}\text{Rn}$  to  
463 subantarctic and Antarctic areas, *Tellus*, 42B, 83-99, 1990.
- 464 Hirsch, R.M., Slack, J.R., and Smith, R.A.: Techniques of trend analysis for monthly water  
465 quality data, *Water Resour. Res.* 18, 107-121, 1982.
- 466 Hirsikko, A., Nieminen, T., Gagné, S., Lehtipalo, K., Manninen, H. E., Ehn, M., Hörrak, U.,  
467 Kerminen, V.-M., Laakso, L., McMurry, P. H., Mirme, A., Mirme, S., Petäjä, T., Tammet, H.,

468 Vakkari, V., Vana, M., and Kulmala, M.: Atmospheric ions and nucleation: a review of  
469 observations, *Atmos. Chem. Phys.*, 11, 767-798, doi:10.5194/acp-11-767-2011, 2011.

470 Ilić, R., Rusov, V.D., Pavlovyh, V.N., Vaschenko, V.M., Hanžič, L., Bondarchuk, Y.A.:  
471 Radon in Antarctica, *Radiat. Meas.*, 40, 415-422, 2005.

472 Jacob, D.J., Prather, M.J., Rasch, P.J., Shia, R.-L., Balkanski, Y.J., Beagley, S.R., Bergmann,  
473 D.J., Blackshear, W.T., Brown, M., Chiba, M., Chipperfield, M.P., de Grandpré, J., Dignon,  
474 J.E., Feichter, J., Genthon, C., Grose, W.L., Kasibhatla, P.S., Köhler, I., Kritz, M.A., Law, K.,  
475 Penner, J.E., Ramonet, M., Reeves, C.E., Rotman, D.A., Stockwell, D.Z., Van Velthoven,  
476 P.F.J., Verver, G., Wild, O., Yang, H., Zimmermann, P.: Evaluation and intercomparison of  
477 global atmospheric transport models using  $^{222}\text{Rn}$  and other short-lived tracers, *J. Geophys.*  
478 *Res.*, 102(D5), 5953-5970, doi:10.1029/96JD02955, 1997.

479 Jones, A.E., Anderson, P.S., Wolff, E.W., Roscoe, H.K., Marshall, G.J., Richter, A., Brough,  
480 N., and Colwell, S.R.: Vertical structure of Antarctic tropospheric ozone depletion events:  
481 characteristics and broader implications, *Atmos. Chem. Phys.*, 10, 7775-7794,  
482 doi:10.5194/acp-10-7775-2010, 2010.

483 Karstens, U., Schmithüsen, D., Schwingshackl, C., and Levin, I.: A process-based  $^{222}\text{Rn}$   
484 flux map for Europe and its verification by long-term observations, to be submitted to ACPD,  
485 2014.

486 König-Langlo, G., King, J.C., Pettré, P.: Climatology of the three coastal Antarctic stations  
487 Dumont d'Urville, Neumayer and Halley, *J. Geophys. Res.*, 103(D9), 10,935-10,946, 1998.

488 Lambert, G., Ardouin, B., and Sanak, J.: Atmospheric transport of trace elements toward  
489 Antarctica, *Tellus*, 42B, 76-82, 1990.

490 Law, R.M., Steele, L.P., Krummel, P.B., and Zahorowski, W.: Synoptic variation in  
491 atmospheric  $\text{CO}_2$  at Cape Grim: a model intercomparison, *Tellus*, 62B, 810-820,  
492 doi:10.1111/j.1600-0889.2010.00470.x, 2010

493 Levin, I., Born, M., Cuntz, M., Langendörfer, U., Mantsch, S., Naegler, T., Schmidt, M.,  
494 Varlagin, A., Verclas, S., and Wagenbach, D.: Observations of atmospheric variability and  
495 soil exhalation rate of radon-222 at a Russian forest site, *Tellus*, 54B, 462-475, 2002.

496 Liu, S.C., McAfee, J.R., and Cicerone, R.J.: Radon 222 and tropospheric Vertical Transport,  
497 J. Geophys. Res., 89(D5), 7291-7297, 1984.

498 Maenhaut, W., Zoller, W.H., Coles, D.G.: Radionuclides in the South Pole Atmosphere, J.  
499 Geophys. Res., 84(C6), 3131-3138, 1979.

500 Mauritsen, T., and Svensson, G.: Observations of stably stratified shear-driven atmospheric  
501 turbulence at low and high Richardson numbers, J.Atmos. Sci., 64, 645-655, 2007.

502 Nazaroff, W.W.: Radon Transport From Soil to Air, Reviews of Geophysics, 30 (2), 137-160,  
503 1992.

504 Pereira, E.B.: Radon-222 time series measurements in the Antarctic peninsula (1986-1987),  
505 Tellus, 42B, 39-45, 1990.

506 Polian, G., Lambert, G., Ardouin, B., and Jegou, A.: Long-range transport of continental  
507 radon in subantarctic and antarctic areas, Tellus, 38B, 178-189, 1986.

508 Porstendörfer, J.: Properties and behaviour of Radon and Thoron and their decay products in  
509 the air, J. Aerosol Sci., 25, No. 2, 219-263, 1994.

510 Schery, S.D. and Huang, S.: An estimate of the global distribution of radon emissions from  
511 the ocean, Geophys. Res. Lett., 31, L19104, doi:10.1029/2004GL021051, 2004.

512 Slemr, F., Brunke, E.-G., Whittlestone, S., Zahorowski, W., Ebinghaus, R., Kock, H.H., and  
513 Labuschagne, C.: <sup>222</sup>Rn-calibrated mercury fluxes from terrestrial surface of southern Africa,  
514 Atmos. Chem. Phys., 13, 6421-6428, doi:10.5194/acp-13-6421-2013, 2013.

515 Stohl, A.: Computation, accuracy and applications of trajectories-a review and bibliography,  
516 Atmos. Environ., 32(6), 947-966, 1998.

517 Stull, R.B.: An Introduction to Boundary Layer Meteorology, Kluwer Academic Publishers,  
518 Dordrecht, Dordrecht, 175-180, 1988.

519 Taguchi, S., Tasaka, S., Matsubara, M., Osada, K., Yokoi, T., and Yamanouchi, T.: Air-sea  
520 gas transfer rate for the Southern Ocean inferred from <sup>222</sup>Rn concentrations in maritime air  
521 and a global atmospheric transport model, J. Geophys. Res. Atmos., 118,  
522 doi:10.1002/jgrd.50594, 2013.

523 Wagenbach, D., Görlach, U., Moser, K., and Münnich, K.O.: Coastal Antarctic aerosol: the  
524 seasonal pattern of its chemical composition and radionuclide content, *Tellus*, 40B, 423-436,  
525 1988.

526 Weller, R., Wöltjen, J., Piel, C., Resenberg, R., Wagenbach, D., König-Langlo, G., and  
527 Kriews, M.: Seasonal variability of crustal and marine trace elements in the aerosol at  
528 Neumayer station, Antarctica, *Tellus*, 60B, 742-752, doi: 10.1111/j.1600-0889.2008.00372.x,  
529 2008.

530 Weller, R., Minikin, A., Wagenbach, D., and Dreiling, V.: Characterization of the inter-  
531 annual, seasonal, and diurnal variations of condensation particle concentrations at Neumayer,  
532 Antarctica, *Atmos. Chem. Phys.*, 11, 13243-13257, doi:10.5194/acp-11-13243-2011, 2011a.

533 Weller, R., Wagenbach, D., Legrand, M., Elsässer, C., Tian-Kunze, X., and König-Langlo, G.:  
534 Continuous 25-years aerosol records at coastal Antarctica – 1: inter-annual variability of ionic  
535 compounds and links to climate indices, *Tellus*, 63B, 901-919, doi: 10.1111/j.1600-  
536 0889.2011.00542.x, 2011b.

537 Wilkening, M.H. and Clements, W.E.: Radon 222 from the Ocean Surface, *J. Geophys. Res.*,  
538 80(27), 3828-3830, 1975.

539 Wyputta, U.: On the transport of trace elements into Antarctica using measurements at the  
540 Georg-von-Neumayer station, *Tellus*, 49B, 93-111, 1997.

541 Zahorowski, W., Griffiths, A.D., Chambers, S.D., Williams, A.G., Law, R.M., Crawford, J.,  
542 and Werczynski, S.: Constraining annual and seasonal radon-222 flux density from the  
543 Southern Ocean using radon-222 concentrations in the boundary layer at Cape Grim, *Tellus*,  
544 65B, 19622, <http://dx.doi.org/10.3402/tellusb.v65i0.19622>, 2013.

545 Zhang, K., Feichter, J., Kazil, J., Wan, H., Zhuo, W., Griffiths, A. D., Sartorius, H.,  
546 Zahorowski, W., Ramonet, M., Schmidt, M., Yver, C., Neubert, R. E. M., and Brunke, E.-G.:  
547 Radon activity in the lower troposphere and its impact on ionization rate: a global estimate  
548 using different radon emissions, *Atmos. Chem. Phys.*, 11, 7817-7838, doi:10.5194/acp-11-  
549 7817-2011, 2011.

## Figure captions

Figure 1. Map of the high latitude Southern Hemisphere showing the locations of the measuring sites discussed in the text.

Figure 2.  $^{222}\text{Rn}$  activity time series based on daily means; red circles refer to summer (JFM) values.

Figure 3.  $^{222}\text{Rn}$  activity time series based on monthly means.

Figure 4. Box plots for the mean seasonality of  $^{222}\text{Rn}$  activity observed from 1995 through 2011. Lines in the middle of the boxes represent sample medians (mean: red line), lower and upper lines of the boxes are the 25<sup>th</sup> and 75<sup>th</sup> percentiles; whiskers indicate the 10<sup>th</sup> and 90<sup>th</sup> percentiles, dots 5<sup>th</sup> and 95<sup>th</sup> percentiles.

Figure 5. Ten-days back trajectories for highest  $^{222}\text{Rn}$  activity concentrations.

Figure 6. Ten-days back trajectories for lowest  $^{222}\text{Rn}$  activity concentrations.

Figure 7. Daily 10-days back trajectories for summer. Shown is the relative (percentage) number of trajectory intersection on a given grid cell (resolution  $1^\circ \times 1^\circ$ ). The left hand plot (a) presents all 10-day back trajectories for  $^{222}\text{Rn}$  activity concentrations above one std of the mean ( $>0.043 \text{ Bq m}^{-3}$ ,  $N = 188$ ), while on the right (b) the corresponding 10-days back trajectories for  $^{222}\text{Rn}$  activity concentrations below one std of the mean ( $<0.013 \text{ Bq m}^{-3}$ ,  $N = 139$ ) are shown.

Figure 8. The same presentation as in Fig. 7, but now for winter: (a) all 10-day back trajectories for  $^{222}\text{Rn}$  activity concentrations above one std of the mean ( $>0.023 \text{ Bq m}^{-3}$ ,  $N = 257$ ) and (b) for  $^{222}\text{Rn}$  activity concentrations below one std of the mean ( $<0.007 \text{ Bq m}^{-3}$ ,  $N = 209$ ).

Figure 9. Relation between CP concentrations presented on (a) linear as well as (b) on logarithmic scale and  $^{222}\text{Rn}$  activity concentrations. Data points correspond to 3-hour means, i.e. the highest available temporal resolution of the measured  $^{222}\text{Rn}$  activity concentrations. The calculated Pearson correlation coefficient is  $r = 0.213$  ( $r^2 = 0.045$ ;  $N = 42434$ ).

Figure 10. Box plots for the mean seasonality of (a)  $^{210}\text{Pb}$  concentration, (b) La concentration, (c) bulk Richardson number  $\text{Ri}_B$ , and (d) SIE for the sector  $20^\circ\text{-}30^\circ$ . For description of the symbols see Fig. 4.

Figure 11. Correlation between  $^{222}\text{Rn}$  activity and SIE (unit:  $10^6 \text{ km}^2$ ) between  $20^\circ\text{E}$  and  $30^\circ\text{E}$  for summer (JFM) based on respecting daily mean values. Regression (blue line) calculated by bivariate Williamson-York method (Cantrell, 2008) with slope =  $-(0.124 \pm 0.028) \times 10^{-6} \text{ Bq m}^{-3} \text{ km}^{-2}$ , intercept =  $(0.028 \pm 0.001) \text{ Bq m}^{-3}$ .

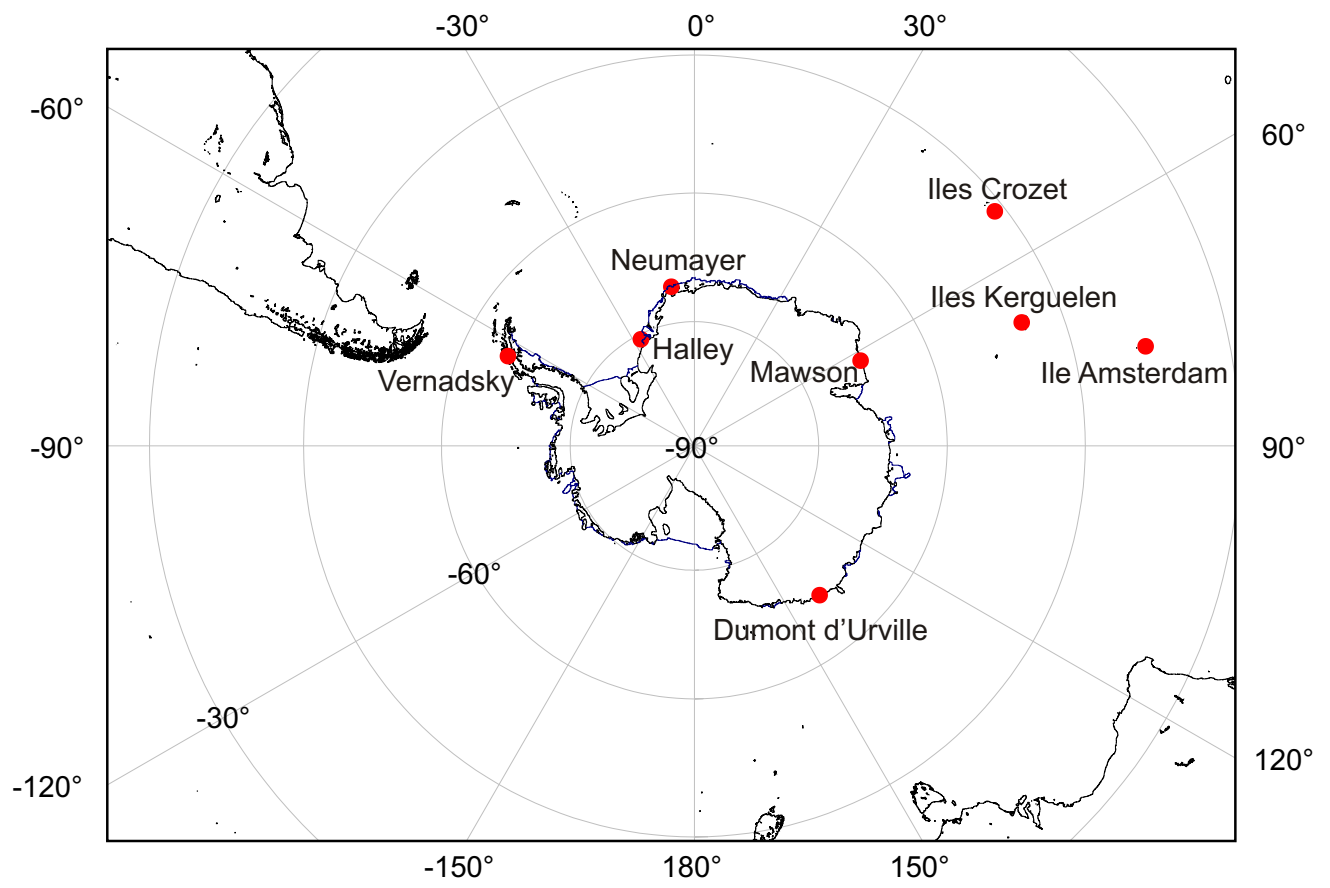


Fig. 1

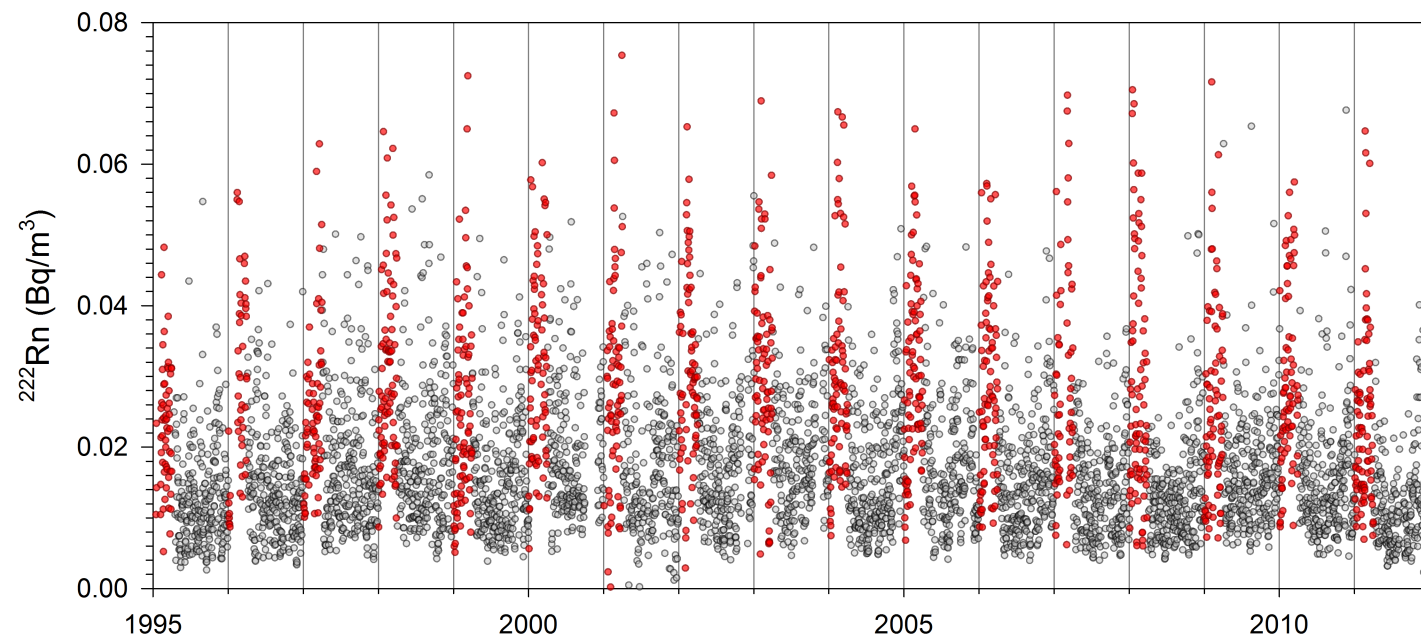


Fig. 2

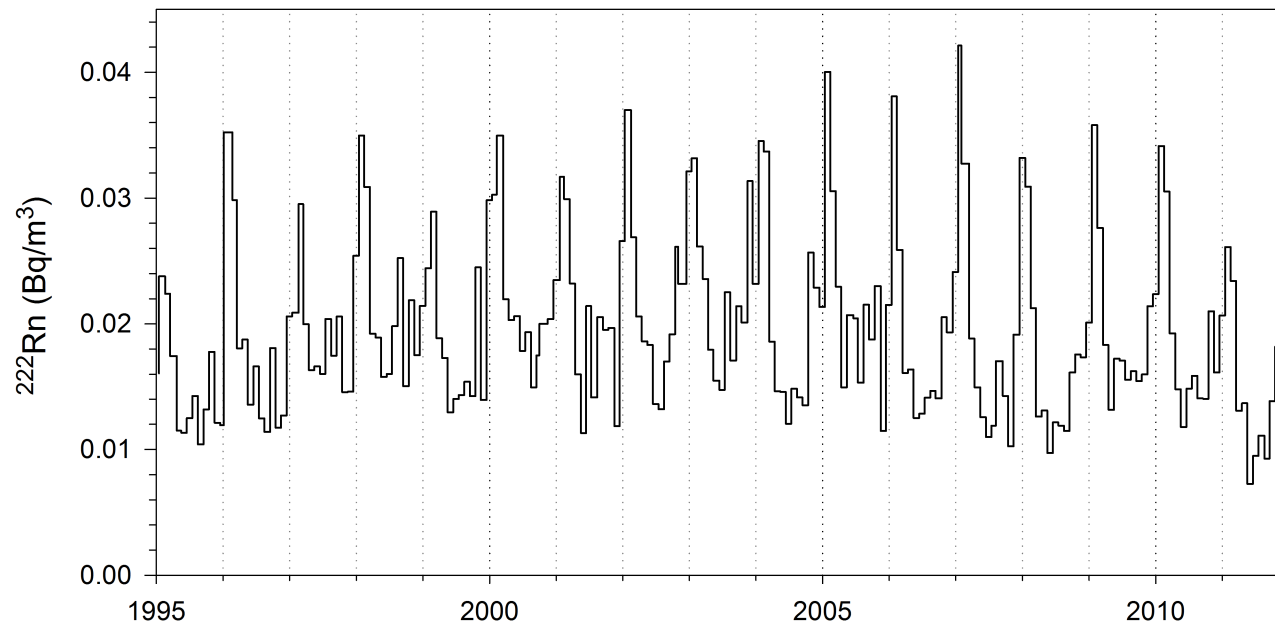


Fig. 3

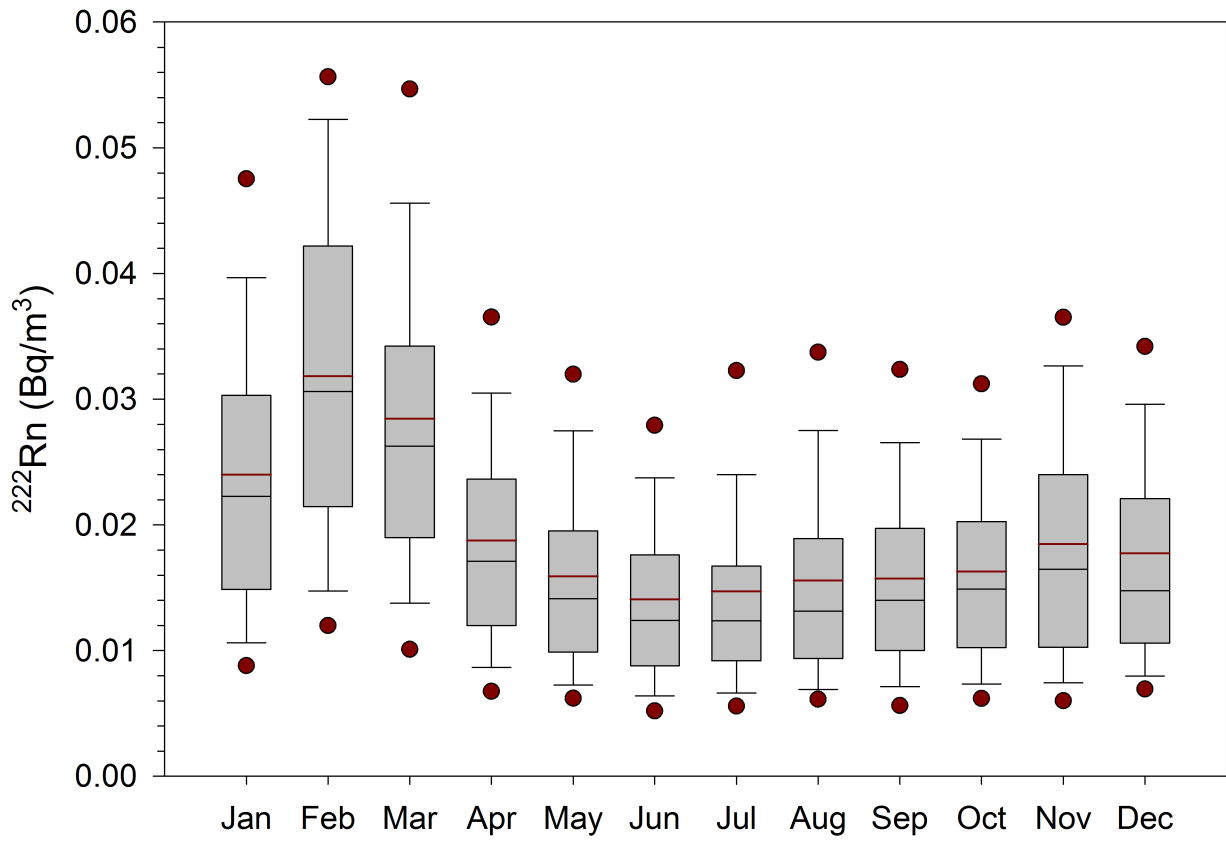


Fig. 4

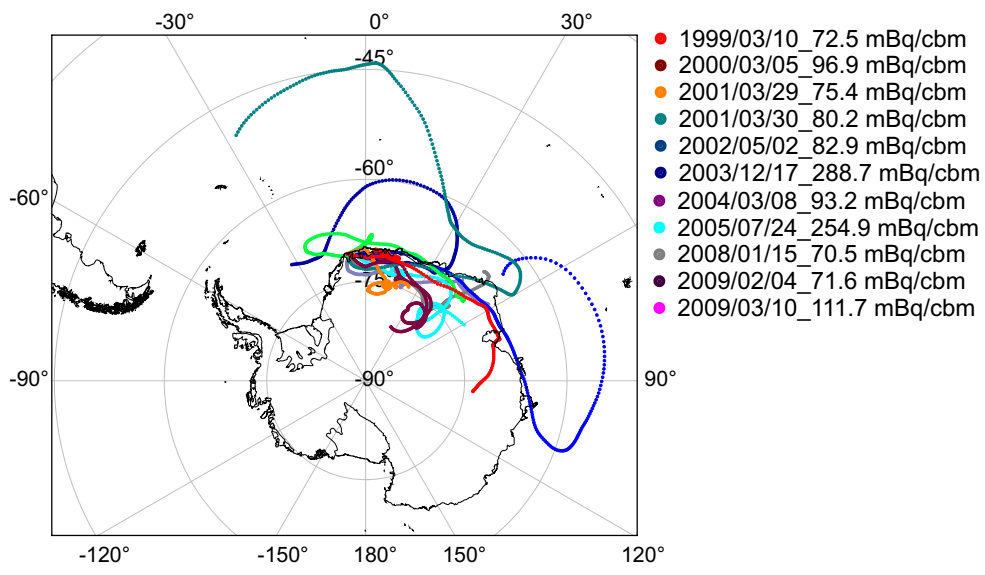


Fig. 5

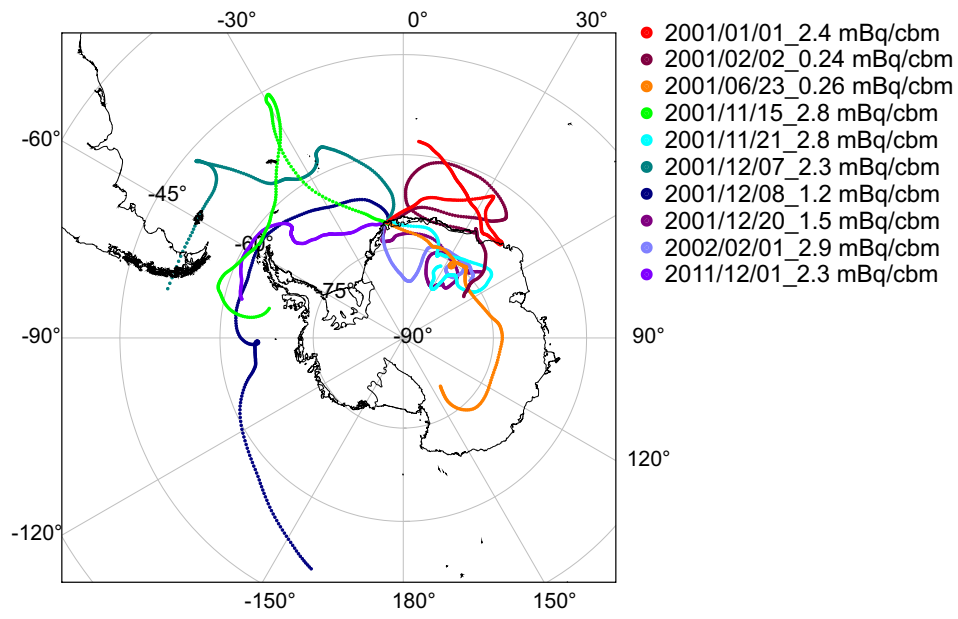


Fig. 6

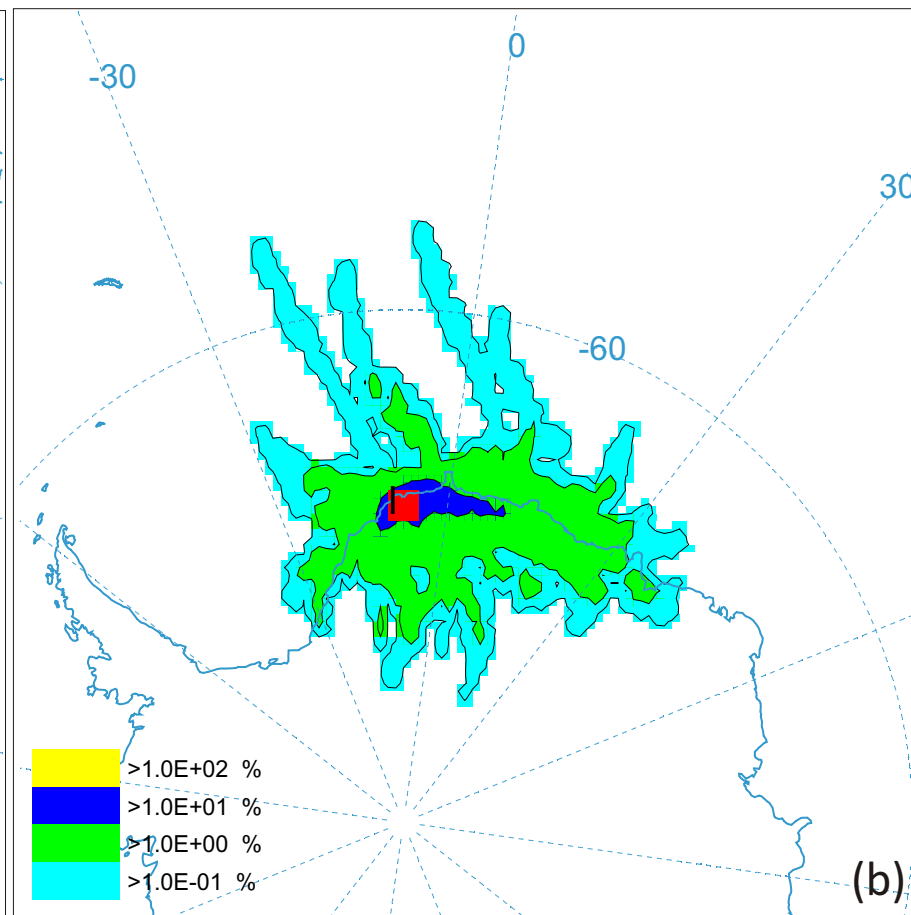
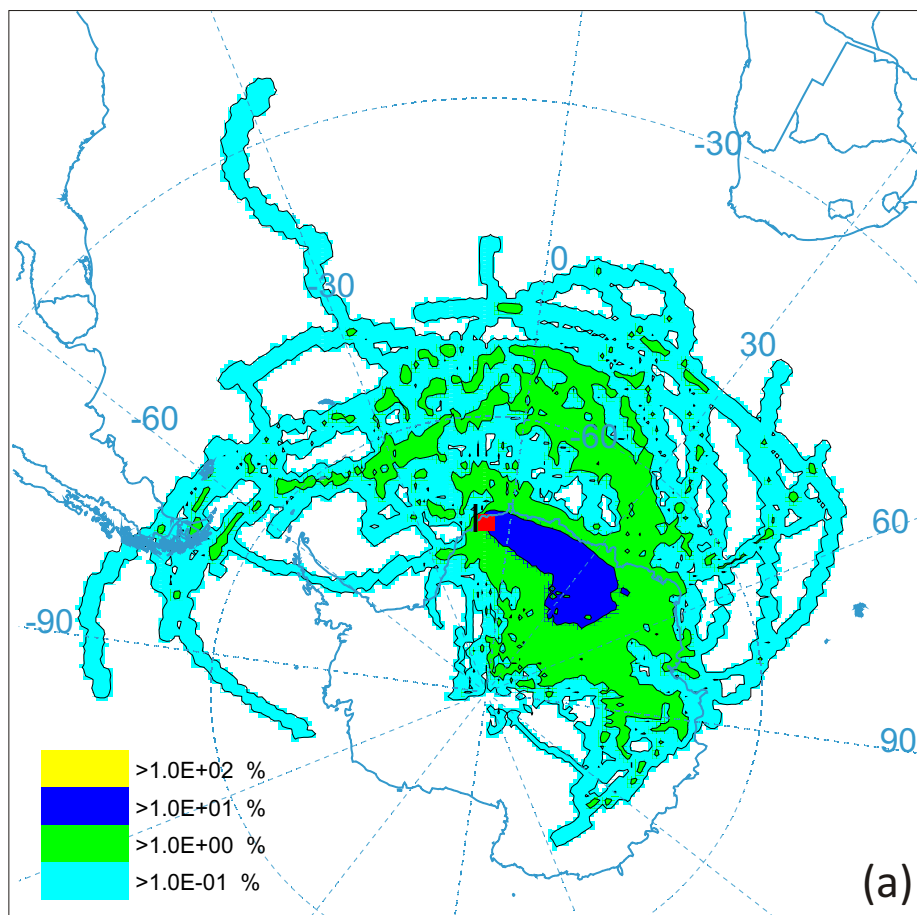


Fig. 7

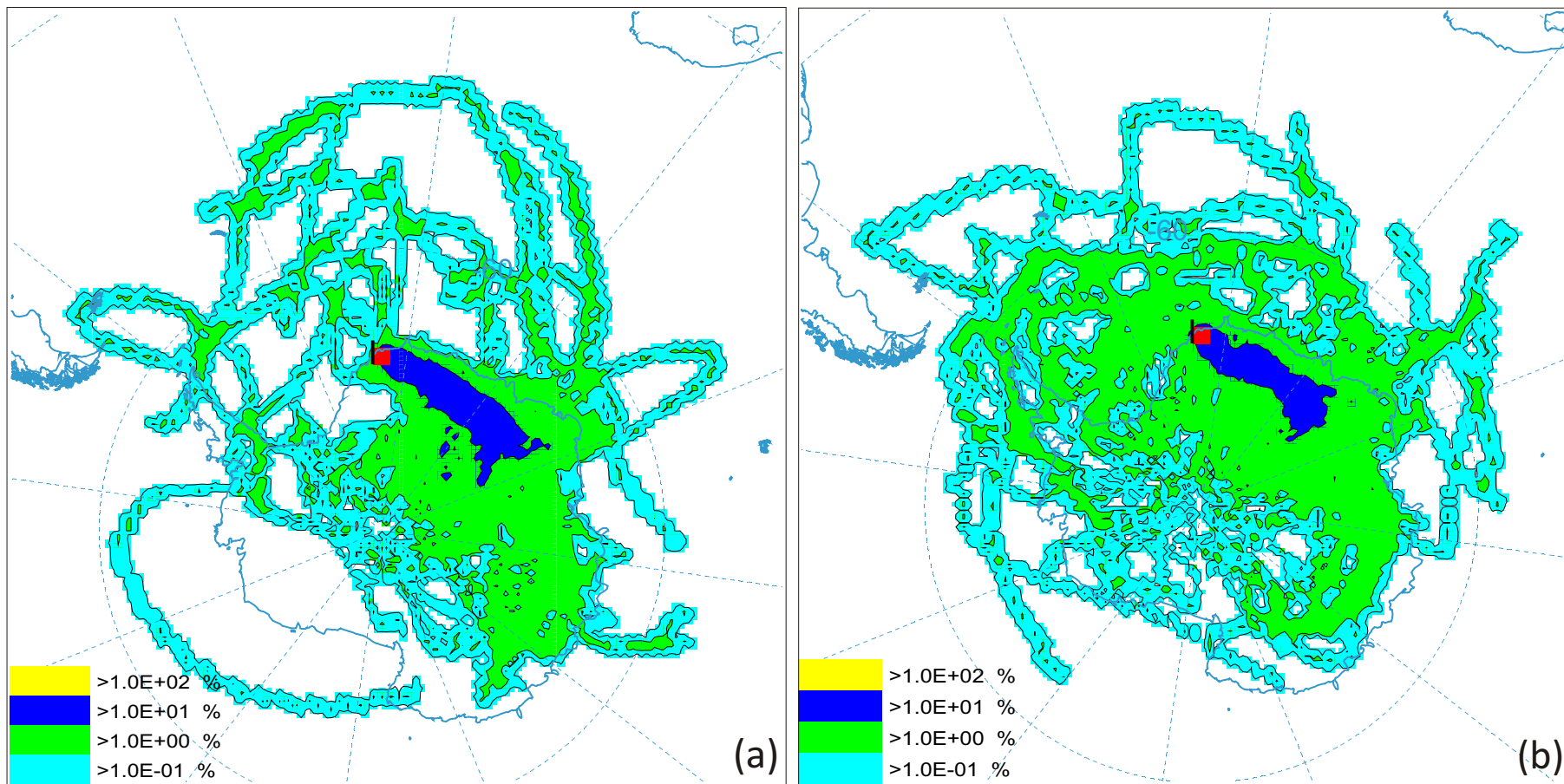


Fig. 8

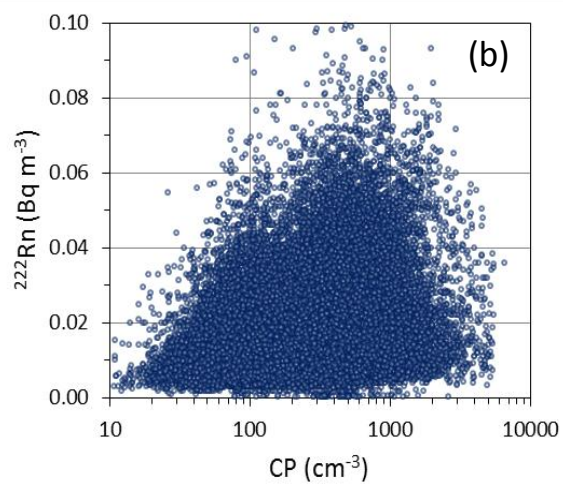
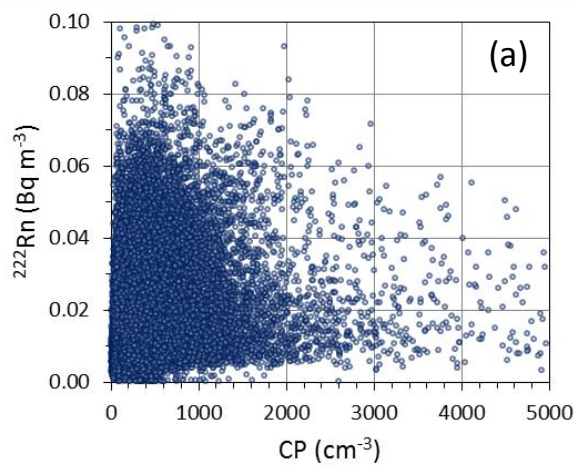


Fig. 9

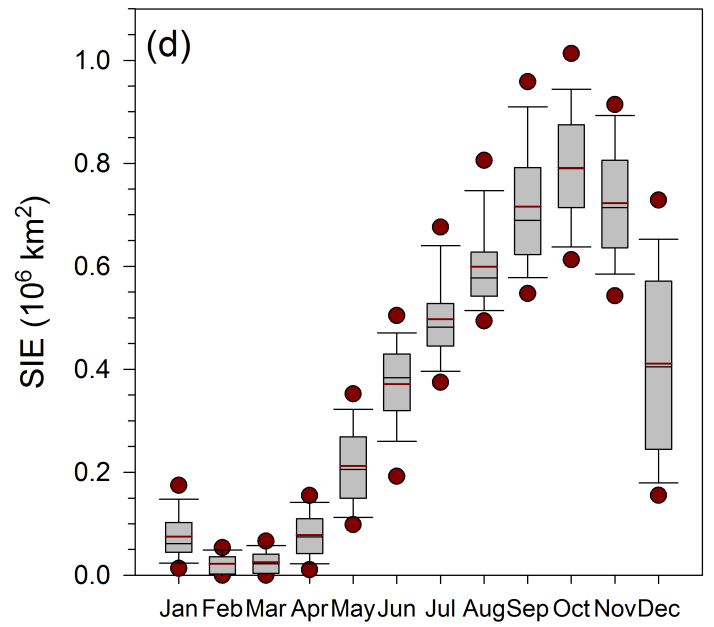
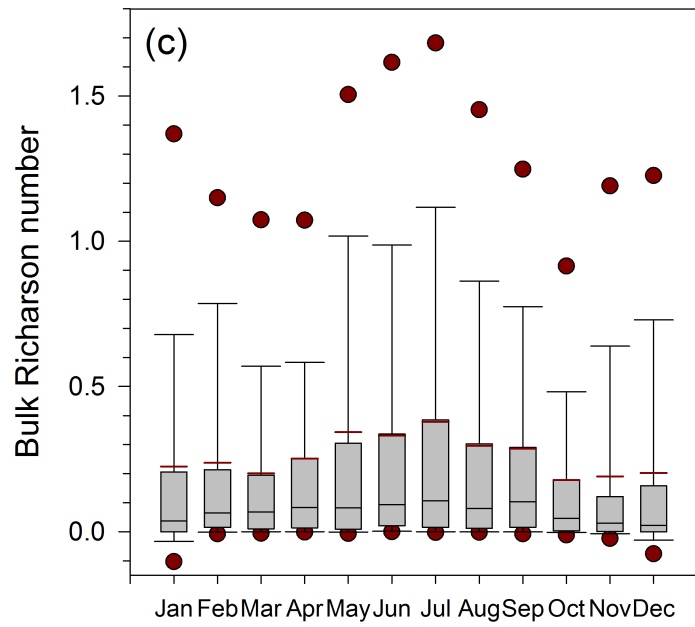
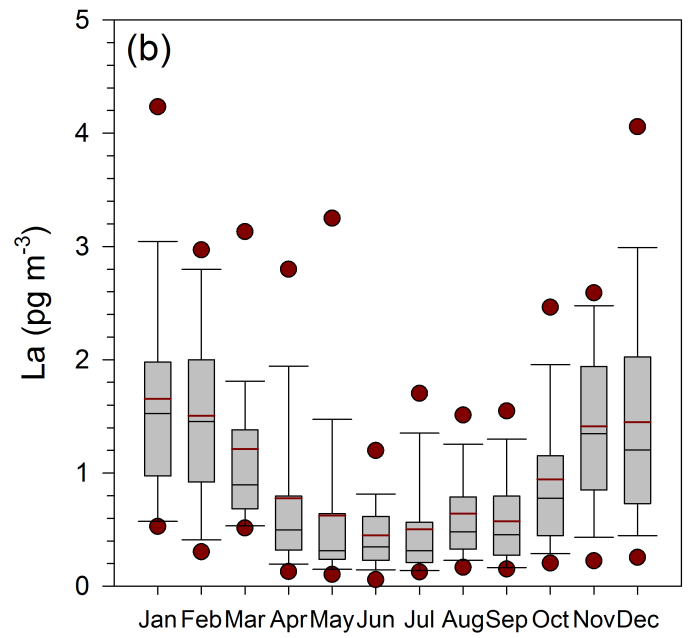
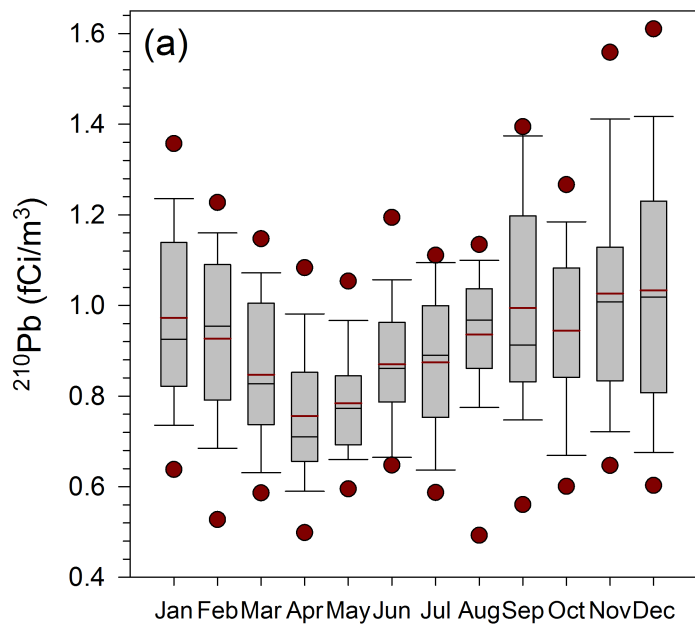


Fig. 10

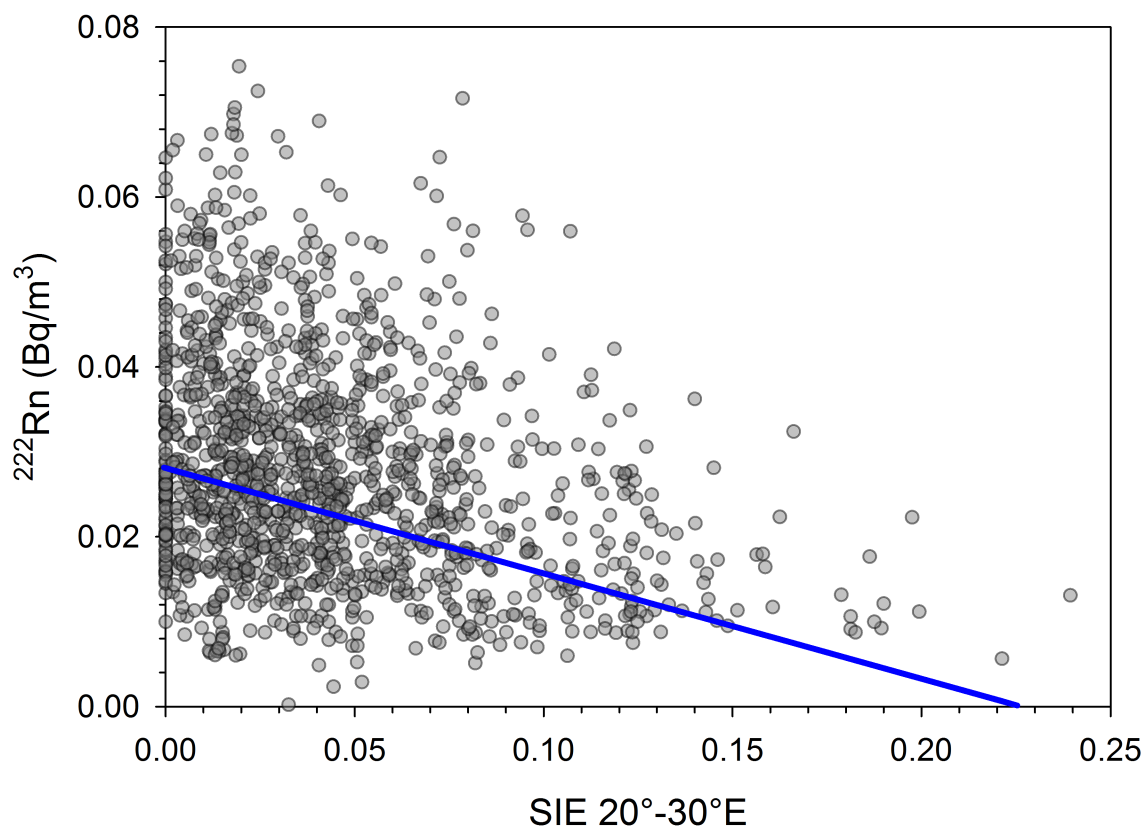


Fig. 11